

CFD COMPARISON FOR THE SARM ROTARY ENGINE WITH A CONVENTIONAL RECIPROCATING OTTO CYCLE ENGINE

¹ Vasilis Gkoutzamanis*, ² Dimitris Mertzis, ¹ Savvas Nikolaidis, ¹ Savvas Savvakis

¹ the SARM Project (www.thesarmproject.com),

Thessaloniki, Greece, N. Zerva 10 Thessaloniki, T :(+30)6978019124, eFax: 7007009099

E-mail: vasilis@thesarmproject.com

²Laboratory of Applied Thermodynamics (lat.eng.auth.gr)

Department of Mechanical Engineering, Aristotle University of Thessaloniki, Greece

KEYWORDS –

SARM, engine, Otto, rotary engine, fuel-air cycle, CFD, 2D, 3D

ABSTRACT –

A new concept rotary engine – the SARM engine – is compared to the conventional reciprocating Otto cycle engine in terms of thermodynamic efficiency and power output. A pseudo-1D fuel-air cycle analysis is performed which is supported by detailed 2D and 3D CFD analyses of both engines.

A pseudo-1D approach of the thermodynamic engine cycle is adopted in order to estimate the thermal efficiency and compare the pressure diagrams of the two engines. The generated tool, which is enriched with data from CFD models, offers rapid sensitivity analysis on the major engine characteristics with minimum time and effort.

The 3D study work's target is the in-depth understanding of the combustion process inside the SARM engine and its comparison with an Otto cycle engine. Both engines were studied with identical initial conditions (engine capacity, inlet pressure, fuel-air ratio).

The analysis results are promising since the SARM engine presents an increase both in thermodynamic efficiency and produced torque. The next step is to optimise the design using the developed tools and proceed to the SARM engine prototype manufacture.

The 2D & 3D geometry model and finite element analysis have been created with the pre-processor ANSA. The CFD analysis has been carried out with ANSYS Fluent and the results are utilised via the μETA post-processor.

TECHNICAL PAPER -

1 INTRODUCTION

In recent years, pronounced attention has been paid to analyze the performance of internal combustion engines such as Otto, Diesel and Wankel, the conventional used types of engines. Otto cycle engine, also known as the four-stroke engine, has been developed by Nikolas Augustus Otto in the 1870's, running today with a thermal efficiency of about 25% to 30% [1]. The well-known high-compression Diesel engine was named after Rudolf Diesel in 1893 and as regards to efficiency levels, they vary from 30% for small high speed engines up to 42-49% for low speed engines [2]. Despite the robustness of the reciprocating engines there were some important disadvantages such as their large number of moving parts, the lower torque produced as regards to the pressure applied on the piston and the increased volume and weight for the amount of power output generated, that gave birth to rotary engines.

Wankel engine, which was so called after Felix Wankel, is a type of internal combustion engine consisting of an eccentric rotary design whose thermal efficiency is around 29% [3]. As compared to the reciprocating engines, it is lighter, simple and more compact. Additionally, it is characterized by lower temperatures developed inside the combustion chamber reducing NOx emissions significantly. The main problems of this kind of engine are the high surface to volume ratio of its combustion chamber at the time of ignition, as well as the blow-by effect appeared at the apex seals [4]. Nowadays, it covers only a small percentage of commercial engines by being mainly implemented in Mazda automobiles.

The abovementioned drawbacks originated the idea of SARM, which is a concentric rotary engine that consists of less moving parts and is characterized by less weight and reduced volume. Moreover, it transfers 100% of the produced pressure applied on the pistons to the engine shaft, expecting so to generate the maximum possible torque of all engine types. SARM engine follows the Atkinson cycle whose thermal efficiency (Equation 1 [5]) can theoretically reach up to 20% higher values than Otto cycle can. However, the thermal efficiency difference between the two engines is expected to be lower than 20% due to the working medium's transfer between SARM's consisting chambers that are described in the following chapter. . The Atkinson cycle can be used in the reciprocating engines as well, in order to increase fuel efficiency. Such an application is found on the Toyota Prius which results in a 12% to 14% better efficiency in terms of power output per fuel consumed than the non-Atkinson engine upon which it is based [6]. The aim of this analysis is to estimate the thermal efficiency of SARM engine's cycle and compare it with Otto cycle.

$$\eta = 1 - (ECR \cdot RC)^{1-\gamma} - \frac{ECR^{1-\gamma} - ECR \cdot (1-\gamma) - \gamma}{(\gamma-1)} \cdot \frac{P_1 V_1}{Q_{in}} \quad \text{Equation 1}$$

Where,

η = thermal efficiency [-]

γ = isentropic expansion factor for ideal gas [-]

ECR = ER / RC [-]

CR = compression ratio [-]

ER = expansion ratio [-]

Q_{in} = heat input [J]

P_1 = inlet pressure [Pa]

V_1 = initial capacity [m³]

2 DESCRIPTION OF THE SARM ENGINE

SARM engine comprises of at least two pistons of different rotation radius, as illustrated in Figure 1. One used for the intake and compression process – called compression piston (1), and at least one used for the combustion and expansion process – called expansion piston (2). The compression piston should have the smallest possible cyclic orbit and thus its rotation radius should be equal or similar to the engine shaft's diameter, while the expansion piston should have the biggest possible cyclic orbit and so its rotation radius is at least twice the size of the engine shaft's diameter.

As far as the chambers are concerned, SARM consists of one compression chamber (3) (CPC) designed to provide the intake and compression process, one combustion chamber (4) (CBC) for providing the combustion and expansion process, as well as one extra chamber, the pressure chamber (5) (PC), placed between the two other chambers with the role to control the communication of the other two through valves (6). The pressure chamber stores air under high pressure charged by the compression chamber and its main role is to minimize the pressure loss appeared during the transfer of the high-pressure compressed air from the compression chamber to the combustion chamber. Besides that, the CFD analysis

showed that its presence makes the combustion chamber's flow field highly turbulent even at low rotational speeds [4].

This effectively ensures a good mixing of the fuel with the combustion air, enforcing also the fuel evaporation process. Moreover it allows, especially at high rotational speeds, the injection process and the fuel-air mixing to last longer, giving more time to the fuel to evaporate and making the mixture more homogeneous.

For more details of how the engine operates, please visit the website:
www.thesarmproject.com



Figure 1 - SARM Engine

3 PSEUDO-1D ANALYSIS

3.1 Introduction

In the case of 1D Analysis, it was difficult to embody the pressure chamber's role, so the calculations were kept as simple as possible, assuming that the compressed air is transferred from the compression chamber to the combustion chamber with no pressure loss. The purpose of the 1D analysis is to develop a tool for engine sensitivity analysis and draft comparisons. It is a starting point that is meant to be further supported by the ongoing and future CFD simulations to increase model reliability.

3.2 The pseudo-1D model

3.2.1 Geometrical dimensions

The geometrical dimensions as well as the common parameters for both models (SARM & Otto) are shown in Table 1.

Table 1- Geometry of both models (pseudo-1D model)

| SARM | | Otto | | |
|---------------------|---------------------------------------|----------|-----------------------------|------------|
| Compression Chamber | Piston Diameter [mm] | 38 | Bore [mm] | 60 |
| | Piston rotation radius [mm] | 100 | Stroke [mm] | 64.7 |
| | Compression Volume [cm ³] | 240 | Capacity [cm ³] | 240 |
| Combustion Chamber | Piston Diameter [mm] | 38 | Connecting Rod Length [mm] | 95 |
| | Piston rotation radius [mm] | 200 | | |
| | Compression Ratio | 11 : 1 | Compression Ratio | 11 : 1 |
| | Speed [rpm] | 1000 rpm | speed | 1000 [rpm] |
| | Heat input [J] | 288 | Heat input [J] | 288 |

The 1D Analysis was elaborated with the help of an Excel file using the functions available in all Internal Combustion Engine books, like Heywood [7], and, in the case of the combustion process, it was described by the Wiebe function using for both engine models $n=2$ and $a=5$. The geometrical dimensions were calculated so that both engines (SARM & Otto) have the same compression ratio (CR=11).

The fuel used for both models is methane since the first target group for SARM is the low/medium speed marine engines and GenSets used in cargo LNG ships, whose fuel is tending to be natural gas.

3.2.2 The 1D Otto model

The Otto engine is studied during the compression, combustion and expansion process (-180 to 180 degrees). The spark ignition timing is at the Top Dead Center (TDC), which means at the angle position of zero degrees while the combustion duration is assumed 35 degrees. The capacity of the engine is 240cm³ and the speed is 1000rpm.

3.2.3 The 1D SARM model

In this model, the capacity of the engine is assumed to be the compression volume, even though this is not the right way to define the capacity of the model, if the pressure chamber is taken into consideration. 2D and 3D simulations have shown that the pressure chamber influences the amount of fuel burnt and so the initial ignition volume and compression volume.

Thus, for the 1D Analysis, the capacity of the engine is the same as its initial compression chamber volume and in this case is 240cm³.

The compression ratio is 11:1, like in the Otto case and the engine's speed is 1000 rpm. The heat input is also 288 J, in order for the two engines to have the same fuel consumption. However, the combustion process duration is shorter than in Otto case (26 degrees, compared to 35 degrees for Otto) because of the higher Reynolds observed during the injection process which allows greater levels of fuel mixing. This is explained in Figure 2 that illustrates the difference between the two engines for the same rotation of the engine shaft. The first point of the curve corresponds to the opening of SARM's upper valves when fuel injection takes place while the end of the curve is when the upper valves close at the ignition point. Reynolds number is nearly 3000 times larger in SARM engine and declines exponentially. The much higher turbulence is caused by the high pressure difference between the pressure chamber and combustion chamber, as well as the much higher SARM piston velocity which facilitates the introduction of the compressed air from the pressure chamber to the combustion chamber by simultaneously ensuring the homogeneous fuel mixture.

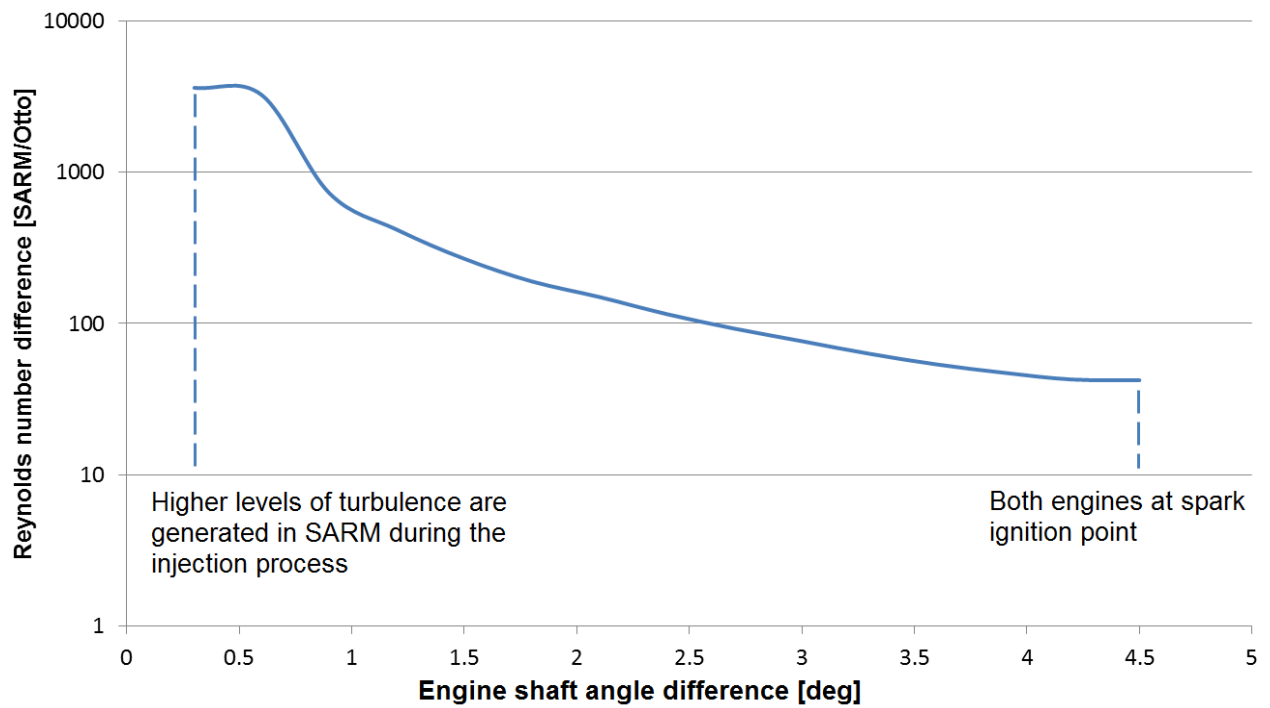


Figure 2 – Reynolds number difference [SARM/Otto]

3.3 Results

The results show that the SARM engine develops lower pressures and this is expected given its volume ratio rate ($dV/d\theta$) during the combustion process (Figure 3). In the case of SARM, the volume ratio is constant and equal to $113.4 \text{ cm}^3/\text{rad}$, while in case of Otto, the ratio increases gradually from zero to a max ratio of $112.24 \text{ cm}^3/\text{rad}$.

The SARM pressure curve includes a small area of steady value (horizontal line). This is the period where the compressed air is transferred from the compression chamber to the expansion chamber.

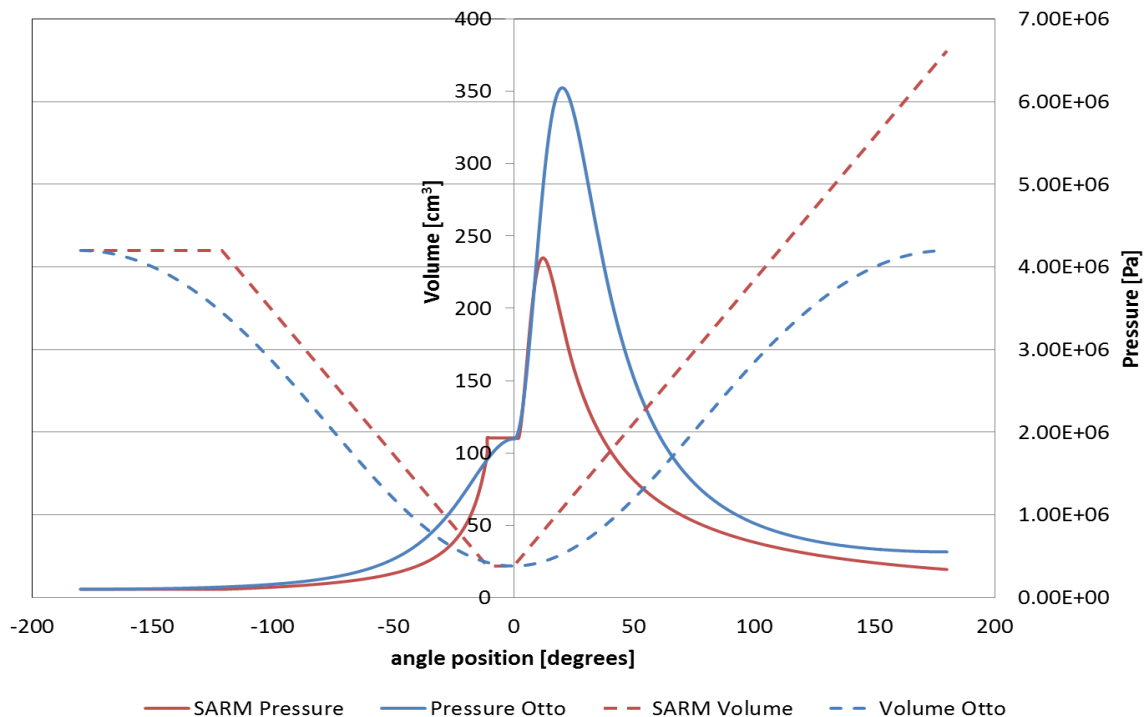


Figure 3 - Pressure and Volume diagram as a function of crank angle position

Although the pressures in SARM are lower, the produced work per cycle is 13.5% higher than Otto, since the accumulated PV product is higher in SARM due to the higher expansion volume compared to the Otto cycle.

Furthermore, a reciprocating engine cannot utilize all the mechanical work produced by the PV changes, as it uses a mechanism to convert the reciprocating motion of the piston to rotating motion at the engine shaft.

Figure 4 compares the force applied on the piston with the coefficient applied on the engine shaft and produces the output torque regarding Otto. Comparing these two forces, they differ by 41% meaning that the same moment could be produced by a 41% lower pressure assuming all the force applied on the piston could be utilized 100% for power generation and SARM does convert the 100% of pressure force applied on the piston to output torque.

Finally, SARM operates similarly to a 2-stroke engine, so it produces this work in half the time than the 4-stroke Otto does. The latter gives a power at every 4 strokes, taking into consideration the intake and exhaust processes, while SARM gives its work in each revolution because the two aforementioned processes take place simultaneously with the compression and expansion process of the previous and next operating cycles. This gives an advantage to SARM by producing twice more power compared to Otto for the specified size which is great for marine engines.

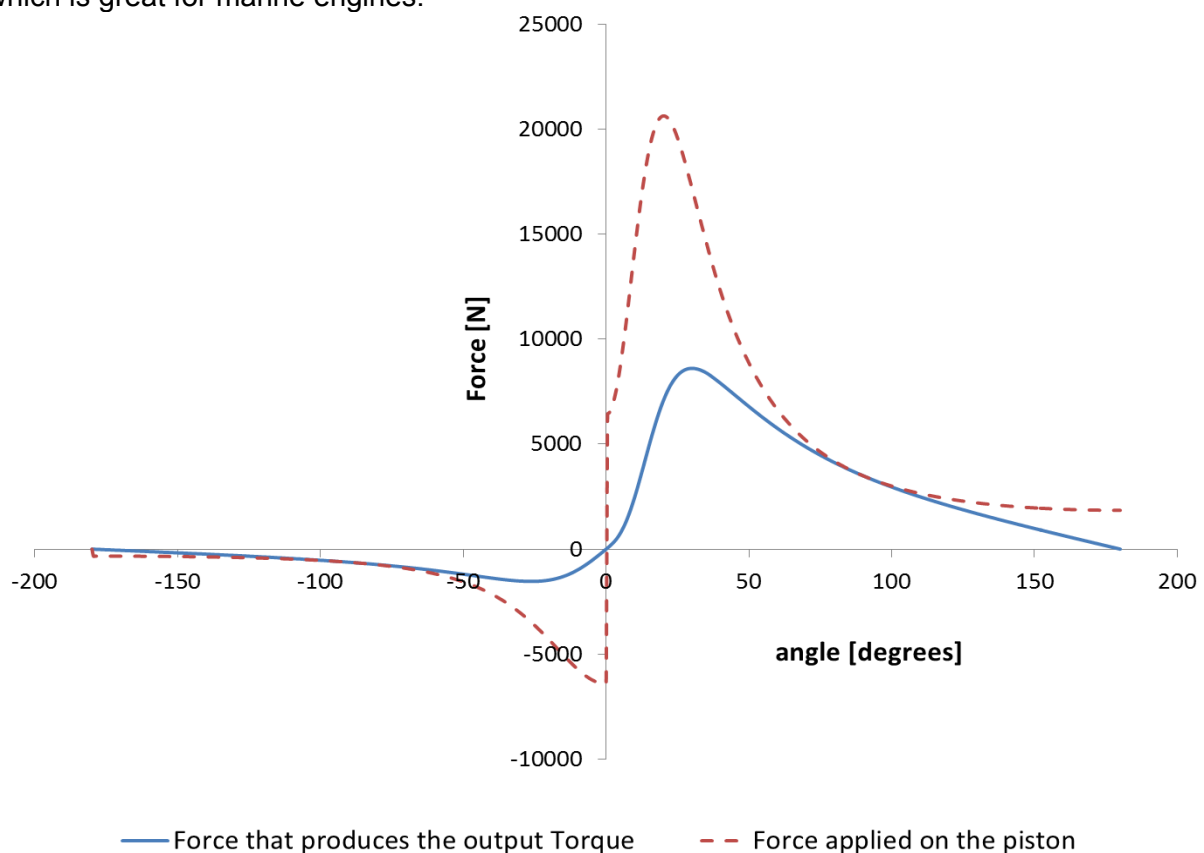


Figure 4 - Comparison of the torque produced by the pressure applied on the piston with the the torque produced on the engine shaft for the Otto engine

3.4 Conclusions

The above analysis concludes that SARM has an advantage compared to Otto. However, the 1D analysis does not take into account the pressure chamber and it simply considers the compressed air to be transferred to the combustion chamber with no pressure losses. Therefore, a more accurate 2D or 3D analysis is important for the abbreviated observation of the pressure chamber's operation. The 2D model serves as a rapid testing tool utilizing CFD in order to determine the optimum engine characteristics (such as valve timing). After the 2D model implementation and finalization of the main characteristics, an elaborated 3D model is utilized in order to retrieve realistic and accurate feedback on the SARM engine concept.

4 2D-ANALYSIS

4.1 Geometry

The 2D CAD and grid for both models have been generated in ANSA v.15.2.3. The dimensions were chosen so that both engines (SARM & Otto) have the same fuel consumption for the same compression ratio.

Table 2- Geometry of both 2D models

| | | SARM | | Otto | |
|---------------------|-----------------------------|-------------------|--------|----------------------------|--------|
| Compression Chamber | Piston Diameter [mm] | 38 | | Bore [mm] | 73 |
| | Piston rotation radius [mm] | 80 | | | |
| Pressure Chamber | Valves closing angle [deg] | 150 | | | |
| | PC Width [mm] | 19.05 (3/4") | | Stroke [mm] | 80.3 |
| | PC Height [mm] | 145 | | | |
| Combustion Chamber | Piston Diameter [mm] | 38 | | Connecting Rod Length [mm] | 100 |
| | Piston rotation radius [mm] | 263 | | | |
| | | Compression Ratio | 11 : 1 | Compression Ratio | 11 : 1 |

4.2 CFD Model

After completing the 2D FE model the numerical model was developed using the commercial CFD solver ANSYS FLUENT. The solution setup was built using for both cases (Otto and SARM) the same options, such as viscosity, fluid properties, solver controls etc.

Pressure-based solver and absolute velocity formulation are the main characteristics of both transient models. The viscosity model in all simulations is the standard k-epsilon model with standard wall functions for near-wall treatment and the premixed turbulent model for combustion. As far as the combustion stroke is concerned, two user-defined functions (UDF) are included in the model in order to define the swirl ratio and the laminar flame speed.

Additional assumptions and input factors are that:

- the working medium is assumed to be atmospheric dry air behaving as an ideal-gas
- The walls of both geometries are assumed adiabatic
- PRESTO! Algorithm for pressure and PISO scheme for Pressure-Velocity coupling
- Both models (SARM & Otto) are run for 1000rpm with the same fuel (methane).

4.3 Results

The following table (Table 3) indicates the results of the two examined cases.

Table 3- 2D models comparison

| 2D | Otto | SARM |
|---|--------|------------------|
| Compression Ratio | 11 : 1 | 11 : 1 |
| Expansion Ratio | 11 : 1 | 22 : 1 |
| Speed [rpm] | 1000 | 1000 |
| Engine capacity [cm ³] | 579.6 | 475.22 (-21.96%) |
| Pressure at compression end [bar] | 28.17 | 27.92 |
| Volume at ignition point [cm ³] | 26.268 | 30.06 (+14.4%) |
| Pressure at ignition point [bar] | 28.17 | 26.02 (-8.2%) |
| Pressure peak at power stroke [bar] | 61.67 | 42.3 |
| Thermal efficiency [%] | 41.76 | 50.1 (+19.97%) |

Both engines were tested at full load (stoichiometric mixture, $\lambda=1$), the same fuel consumption and the same Compression Ratio (CR). As it is observed in Table 3, Otto has 21.96% bigger engine capacity than SARM. The presence of SARM's intermediate pressure chamber added a supplementary amount of air mass inside the combustion chamber and, as both engines were compared in terms of the same fuel consumption, Otto's capacity had to be increased accordingly and render its fuel mass similar to SARM's.

Although the SARM engine is characterized by lower ignition pressure (26.02 bar compared to 28.17 bar of Otto), and a lower pressure peak during the power stroke, it shows 19.97% higher thermal efficiency because of the greater expansion ratio (22:1).

The P-V diagram in Figure 5 shows that despite the lower developed pressures in SARM, the latter produces higher work.

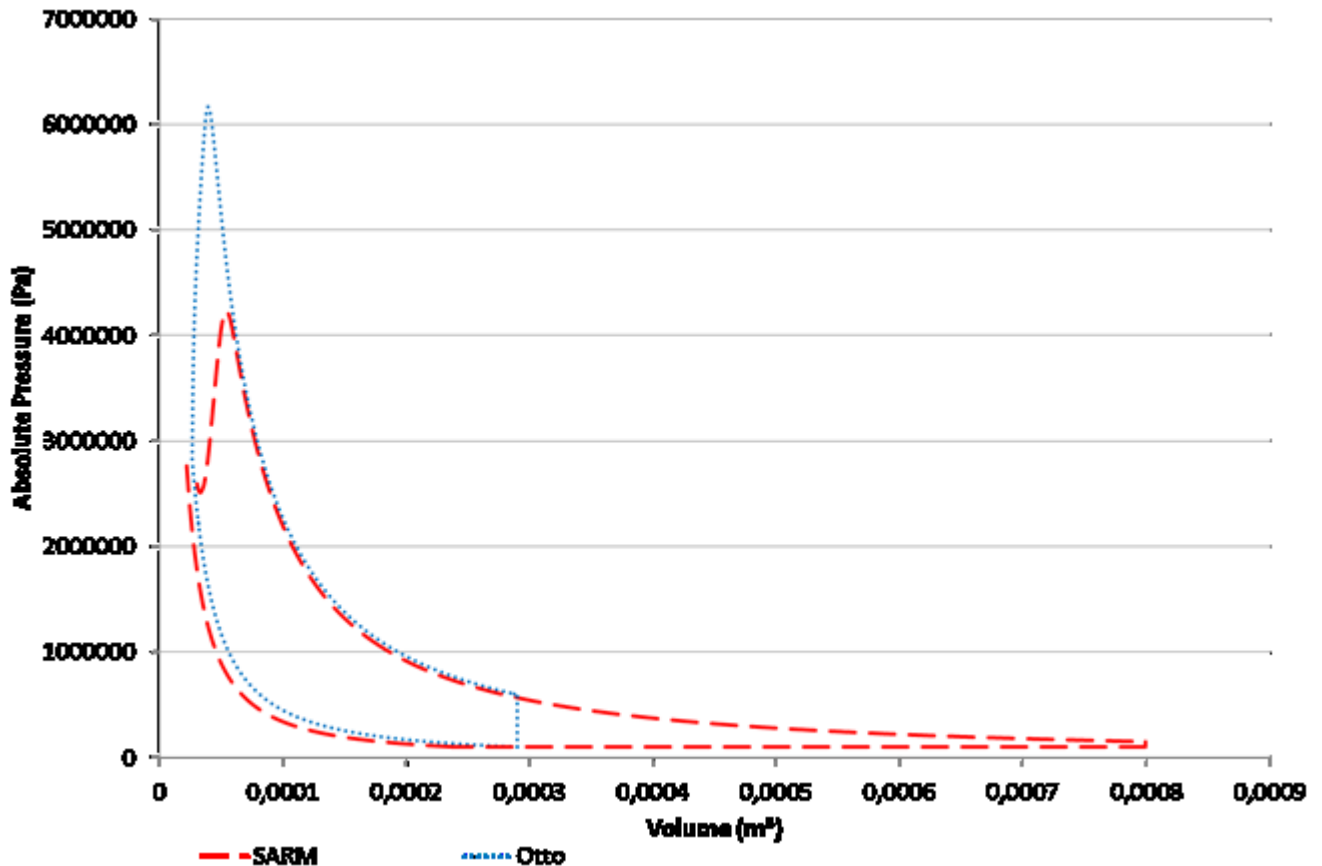


Figure 5 – PV diagrams of the 2D models

Furthermore, Figure 6 shows the flame propagation in both engines. 6a is defined as the zero point ($t_1=0$ sec) of the comparison between the two models and indicates when the ignition takes place. It refers to the position where the Otto piston is at its top dead centre point (TDC) with its crank angle at 360 degrees, while in SARM case the valves have just closed. The examination here is based on how the flame propagates for the same Δt and the same $\Delta\phi$. Figure 6b demonstrates the combustion progress variable in both cases for $\Delta t=0.1$ sec and $\Delta\phi=6$ deg of the engine shaft in both engines.

SARM is characterized by improved flame propagation by means of:

- a highly turbulent flow field inside the combustion chamber caused by the pressure difference ΔP between the pressure- and combustion-chamber, when the valves are open, as well as by the high velocity of the combustion piston, even when the valves are closed.
- geometry of the combustion chamber that approximates the shape of a cube allowing the propagation to be equal in all directions.

Finally, in Figure 6c, the combustion process is complete in Otto and it is almost complete in SARM (more than 98% of the fuel-air mixture is burnt).

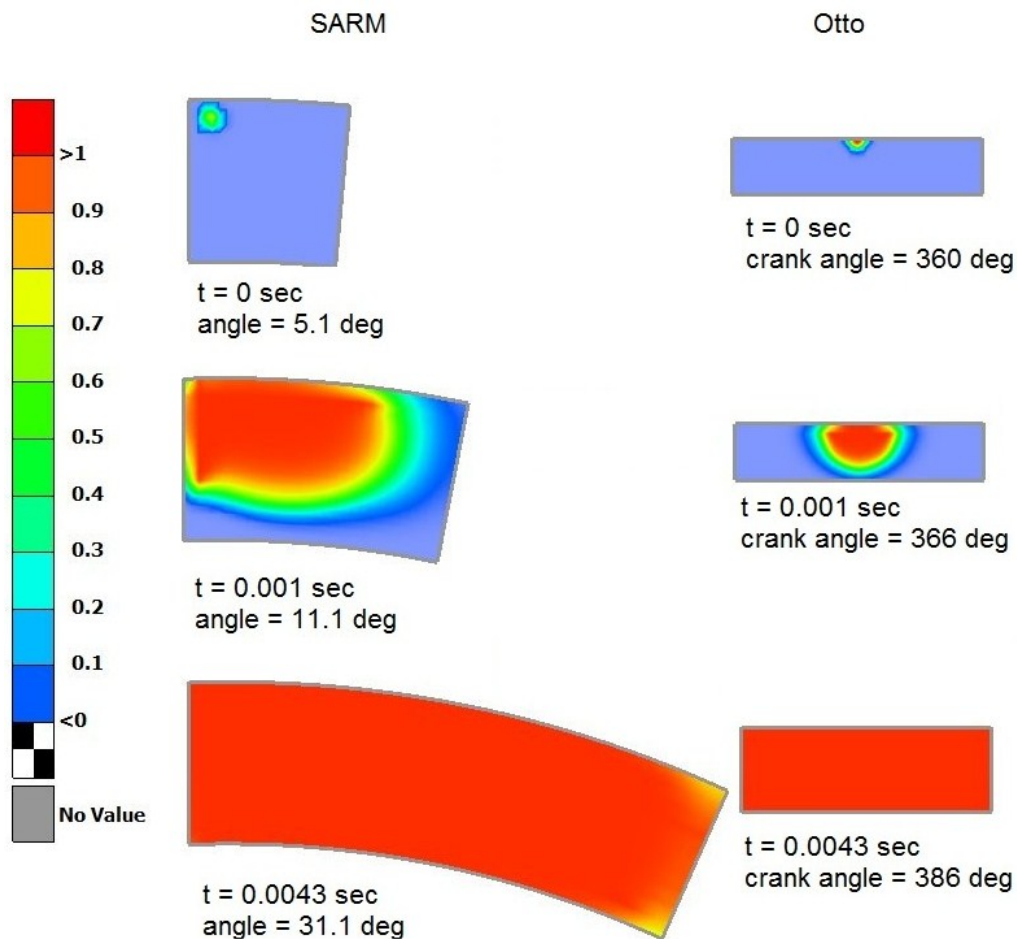


Figure 6 – Progress variable of both 2D models

4.4 Conclusions

A two dimensional analysis offers a swift estimation of the model by taking into account the pressure chamber and valve timing as well. However, the solver used in 2D space is planar and this leads to significant discrepancies from the actual geometry which involves cylindrical chambers and a pressure chamber with a smaller diameter than the other two chambers. Fluent sets a Z-extrusion for all 2D faces at the same distance, in order to define the third dimension for its calculations. So, the hypothetical geometry consists of rectangular shaped chambers and the solver functions are calculated in the 2D plane and hence the volumetric surroundings of the cylindrical volumes are missed. Therefore, the results are not realistic and the analysis should proceed with a more accurate 3D geometry consisting of cylindrical chambers.

5 3D-ANALYSIS

5.1 Geometry

5.1.1 3D – Cylindrical Chambers

The final dimensions of the 3D geometries for SARM, and Otto as well, are shown in Table 4. The choice of 5/4' for the inner diameter of the cylindrical pressure chamber was determined by the dimensions of commercial valves. All valves in the market are designed to fit in pipes and tubes, so the design of the pressure chamber had to be in line with the market's available sizes.

Additionally, three different cases were examined based on the compression ratio used in each one, in order to connect and compare the 2D with the 3D case. The first 3D approach examines a 6:1 compression ratio while the second analysis considers a case that consists of a 10:1 compression ratio. Finally, as methane is the primary compound of natural gas and has been used for the purposes of this case study, it allows the Otto case to be further examined at a 13:1 ratio. On the other hand, SARM is characterized by better cooling conditions and direct fuel injection that minimizes the risk of auto-ignition and hence it can be compressed up to 16:1.

Table 4 – Geometries of both 3D models for all three cases

| | | SARM | | Otto | |
|---------------------|-----------------------------|-------------------|--------|----------------------------|--------|
| Compression Chamber | Piston Diameter [mm] | 38 | | Bore [mm] | 60 |
| | Piston rotation radius [mm] | 80 | | Stroke [mm] | 65 |
| Pressure Chamber | Valve closing angle [deg] | 170 | | Connecting Rod Length [mm] | 95 |
| | PC inner diameter [mm] | 31.75 (5/4') | | | |
| | PC Height [mm] | 145 | | | |
| Combustion Chamber | Piston Diameter [mm] | 38 | | | |
| | Piston rotation radius [mm] | 263 | | | |
| | | Compression Ratio | 6 : 1 | Compression Ratio | 6 : 1 |
| | | SARM | | Otto | |
| Compression Chamber | Piston Diameter [mm] | 38 | | Bore [mm] | 71 |
| | Piston rotation radius [mm] | 80 | | Stroke [mm] | 78 |
| Pressure Chamber | Valve closing angle [deg] | 170 | | Connecting Rod Length [mm] | 100 |
| | PC inner diameter [mm] | 31.75 (5/4') | | | |
| | PC Height [mm] | 145 | | | |
| Combustion Chamber | Piston Diameter [mm] | 38 | | | |
| | Piston rotation radius [mm] | 263 | | | |
| | | Compression Ratio | 10 : 1 | Compression Ratio | 10 : 1 |
| | | SARM | | Otto | |
| Compression Chamber | Piston Diameter [mm] | 38 | | Bore [mm] | 86 |
| | Piston rotation radius [mm] | 80 | | Stroke (mm) | 95 |
| Pressure Chamber | Valve closing angle (deg) | 170 | | Connecting Rod Length [mm] | 140 |
| | PC inner diameter [mm] | 31.75 (5/4') | | | |
| | PC Height [mm] | 145 | | | |
| Combustion Chamber | Piston Diameter [mm] | 38 | | | |
| | Piston rotation radius [mm] | 263 | | | |
| | | Compression Ratio | 16 : 1 | Compression Ratio | 13 : 1 |

Figures 7 and 8 demonstrate the geometries and solid parts that have been used for the simulations. Both geometries and finite element (FE) models were designed by ANSA using pure hexahedral mesh generated by the Hexa Block tools.

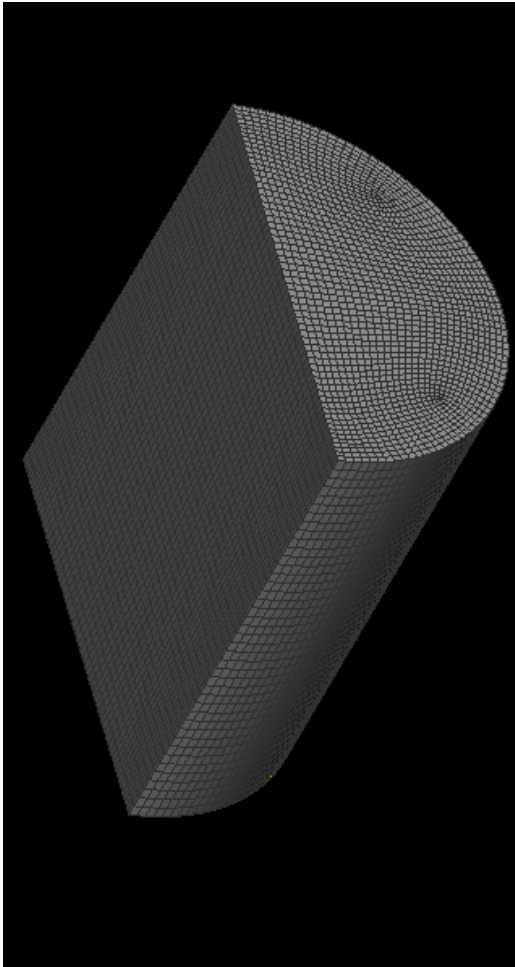


Figure 7 - Otto 3D geometry

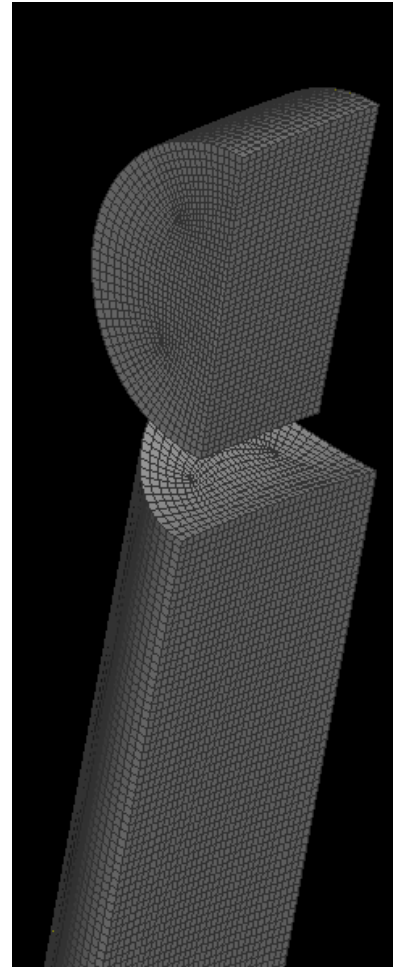


Figure 8 – part of the SARM 3D geometry

5.2 CFD Model

The 3D model follows the exact assumptions and initial conditions as in 2D case (Table 5).

Table 5 - 3D CFD Model

| Problem Setup | | Solution | |
|----------------------|-----------------------|----------------------------|---------|
| Solver type | Pressure-Based | Pressure-Velocity Coupling | PISO |
| Time | Transient | | |
| Velocity Formulation | Absolute | Pressure | PRESTO! |
| Viscous | k-e, standard Wall Fn | | |
| Species | Premixed Combustion | | |
| Walls | Adiabatic | | |
| Density | Ideal gas | | |

5.3 Results

As shown in Figure 9, the 3D simulations confirm the assumption mentioned in the 2D results. The flame propagation inside the SARM engine is higher due to increased levels of turbulence. Pictures demonstrate three different snapshots of the combustion stroke for both engines with the same time and engine shaft angle deviation. Additionally, the SARM engine is characterized by better air-fuel mixing due to the higher turbulence inside the combustion chamber.

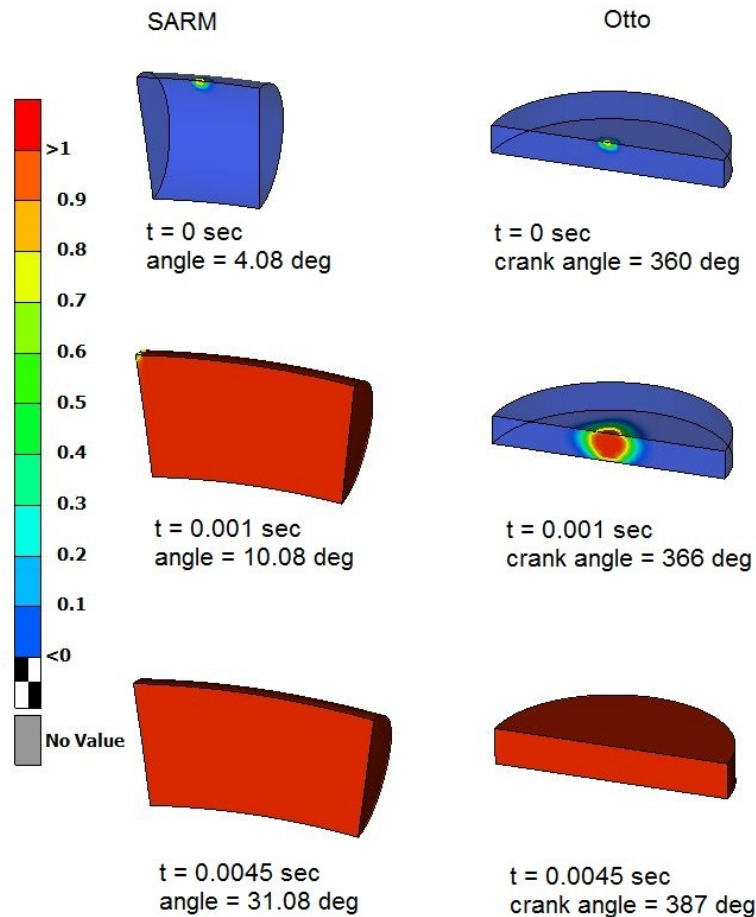


Figure 9 – Progress variable of both 3D models

Both cases are simulated with adiabatic walls and the piston is assumed to be sealed with no leakages. The 3D results show that SARM has a better thermal efficiency with a lower pressure peak during the power stroke which is a desirable aspiration for the engine's operation. That means the materials used to fabricate the engine parts are subject to lower stresses and strains.

An increased thermal efficiency of up to 12.24% -for a 6:1 compression ratio- is calculated from the SARM 3D simulations and is validated by the Atkinson cycle as the latter can reach up to 20% higher thermal efficiencies than Otto cycle does.

The hereunder results indicate that the performance of the SARM engine is prominent as compared to a conventional reciprocating Otto engine (Table 6).

| | 3D | Otto | SARM |
|---|----|--------|---------------|
| Compression Ratio | | 6 : 1 | 6 : 1 |
| Expansion Ratio | | 6 : 1 | 22 : 1 |
| Speed [rpm] | | 1000 | 1000 |
| Engine capacity [cm ³] | | 473.8 | 473.6 |
| Pressure at compression end [bar] | | 12.879 | 12.826 |
| Volume at ignition point [cm ³] | | 76.04 | 88.92 |
| Pressure at ignition point [bar] | | 12.879 | 12.04 |
| Pressure peak at power stroke [bar] | | 56.63 | 29.05 |
| Max. Temperature at power stroke [K] | | 2959 | 2466 |
| Generated work [Joule] | | 306.7 | 335.7 |
| Thermal efficiency [%] | | 38.4 | 43.1(+12.24%) |

The temperatures developed inside the combustion chamber of SARM engine are lower than those of the Otto engine (Table 6). This is a great advantage for SARM as it necessitates lower cooling loads, because the temperature difference between the combustion chamber and the environment is lower. Moreover, this difference is expected to be even lower when the engine will be tested in real conditions as more losses will be generated with the addition of cooling effects and leakages (Figure 10).

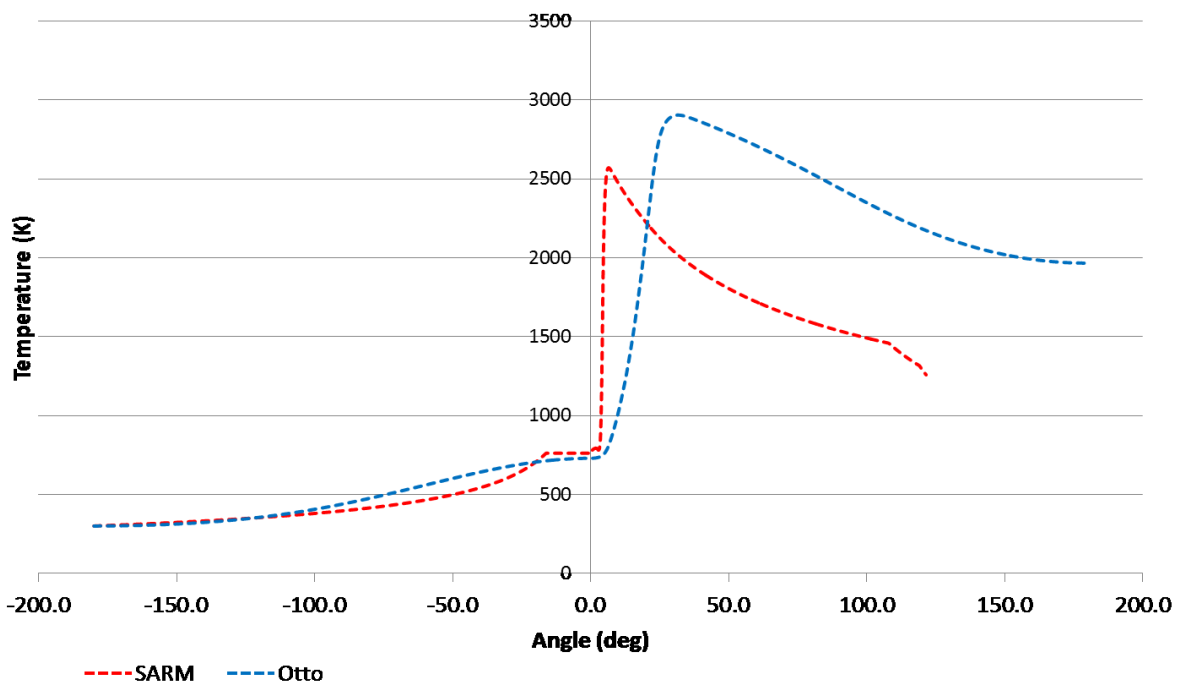


Figure 10 – Temperatures developed

Finally, the P-V diagrams (Figure 11 normal scale, Figure 12 logarithmic scale) illustrate schematically the produced work in each case.

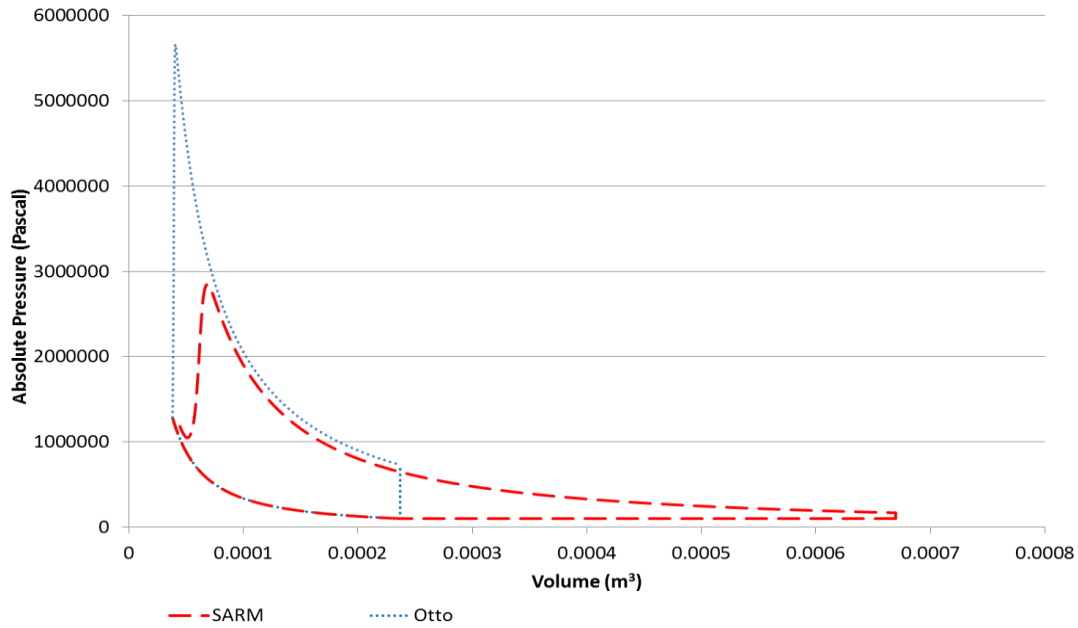


Figure 11 – (6:1) PV Diagram, normal scale

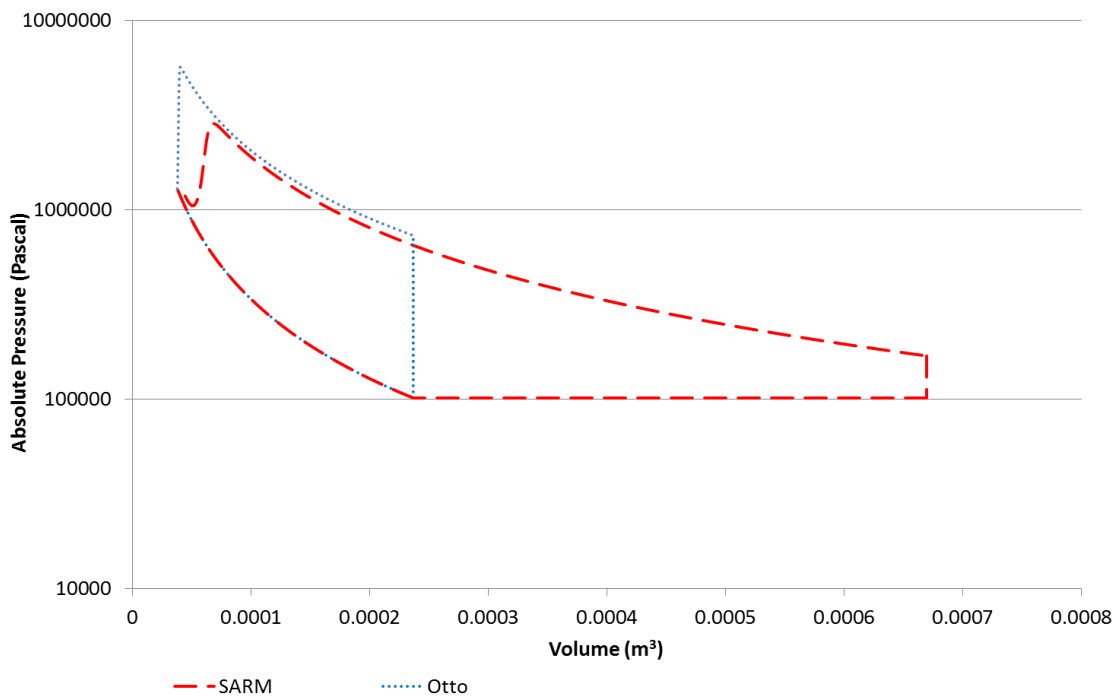


Figure 12 – (6:1) PV Diagram, logarithmic scale

The investigation examines two more cases as already noted at the beginning of this chapter. In general, the increment of compression ratio can improve its thermal efficiency [8]. This is validated by the CFD results of the two last cases. The results of the first case consisting of a 10:1 compression ratio are shown in Table 7, while Table 8 interprets the output results of Otto and SARM for compression ratios of 13:1 and 16:1, respectively.

Table 7 – Results [10:1]

| 3D | Otto | SARM |
|---|--------|-----------------|
| Compression Ratio | 10 : 1 | 10 : 1 |
| Expansion Ratio | 10 : 1 | 22 : 1 |
| Speed [rpm] | 1000 | 1000 |
| Engine capacity [cm ³] | 688 | 473.6 |
| Pressure at compression end [bar] | 24.6 | 24.3 |
| Volume at ignition point [cm ³] | 66.8 | 80.108 |
| Pressure at ignition point [bar] | 24.6 | 22.114 |
| Pressure peak at power stroke [bar] | 78.87 | 49.4 |
| Max. Temperature at power stroke [K] | 2904 | 2569 |
| Generated work [J] | 509.7 | 579.2 |
| Thermal efficiency [%] | 46.16 | 53.12 (+15.07%) |

Table 8 – Results [13:1 – 16:1]

| 3D | Otto | SARM |
|---|--------|----------------|
| Compression Ratio | 13 : 1 | 16 : 1 |
| Expansion Ratio | 13 : 1 | 22 : 1 |
| Speed [rpm] | 1000 | 1000 |
| Engine capacity [cm ³] | 932 | 473.6 |
| Pressure at compression end [bar] | 35.3 | 44.1 |
| Volume at ignition point [cm ³] | 71.4 | 76 |
| Pressure at ignition point [bar] | 35.3 | 39.3 |
| Pressure peak at power stroke [bar] | 86.9 | 79.8 |
| Max. Temperature at power stroke [K] | 2877 | 2633 |
| Generated work [J] | 727 | 883.9 |
| Thermal efficiency [%] | 47.3 | 56.7 (+19.87%) |

Moreover, one would notice that the Otto engine capacity increases considerably when higher compression ratios are used. As mentioned earlier where the SARM's operating principle was described, the initial conditions inside the pressure chamber are the same with the thermodynamic conditions inside the compression chamber at the end of compression process. Consequently, the pressure chamber's initial pressure and temperature increases when the compression ratio increases. Thus, the amount of air-fuel mass concentrated inside the combustion chamber of SARM engine is also increased because the density of the air trapped in the pressure chamber adds an extra amount of air at the combustion chamber. In order to keep the fuel consumption the same for both engines, the volume of Otto engine should be increased correspondingly.

Finally, the thermal efficiency of SARM engine is also increased in both cases with the first one (10:1) reaching up to 15% and 19.9% for the second (13:1 – 16:1). Once again, the temperatures observed in Otto engine are higher and require higher loads for cooling the engine.

The three cases are summarized in the PV diagram below (Figure 13).

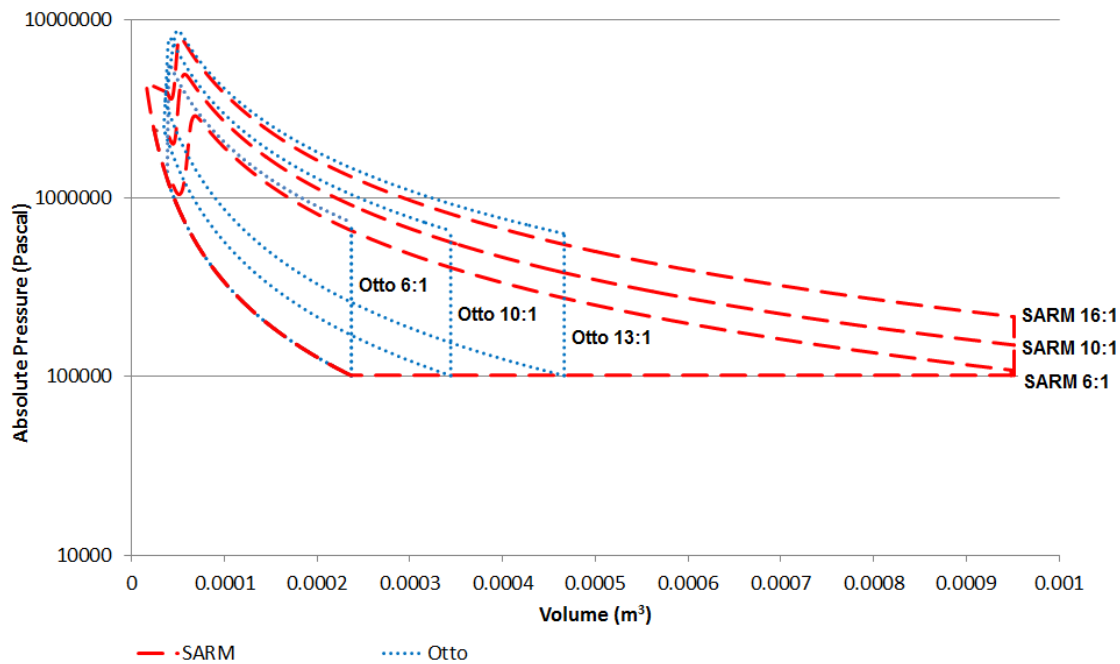


Figure 13 – PV diagram for all cases, logarithmic scale

6 CONCLUSIONS

The analysis of the final optimized configuration shows a 12 - 19% improvement of SARM's thermal efficiency in all analyses (0D, 2D & 3D). So, even though SARM is characterized by lower pressures and temperatures, the initial expectation that the Atkinson cycle used in SARM engine will provide lower fuel consumption compared to Otto engines is confirmed.

The increase in thermal efficiency is within the acceptable limits of an engine that operates with the Atkinson cycle, which theoretically allows up to 20% increase of the thermal efficiency compared to Otto cycle.

Regarding power output, SARM transfers 100% of the produced pressure applied on the pistons to the engine shaft and as a result it generates higher torque compared to reciprocating engines. The latter can take advantage only of the 60% of the applied pressure on the pistons because of the mechanism that converts the reciprocating motion to rotating.

Last but not least, the combustion process in the SARM engine is rapid compared to the conventional SI engine due to increased levels of turbulence which enhances the faster flame propagation. On the other hand, the fast expansion of the combustion volume traps more heat inside the working medium and so less heat has to be removed by the cooling system. Thus, the cooling losses are lower during the first degrees of expansion, where the temperature difference between the chamber and the environment is the highest.

Compression and expansion are assumed to be adiabatic with no leakages. The future work of this analysis is to perform an analysis with higher compression ratios by taking into account the losses from leakages in compression and combustion chamber for both engines and additionally, to measure the differences in peak pressure and temperature if cooling effects are taken into consideration.

7 ACKNOWLEDGEMENTS

The authors would like to thank BETA CAE SYSTEMS S.A for allowing them to use for free ANSA & μETA for the R&D purposes of this paper as well as for giving them the opportunity to present their research in the 6th BETA CAE International conference.

REFERENCES

- (1) "Engineering Thermodynamics" – P.K.Nag, McGraw Hill Education, Fifth edition (2013)
 - (2) "Wealth from waste – Trends and technologies" Banwari Lal, Priyangshu M. Sarma The Energy and Resources Institute (TERI), Third edition (2011)
 - (3) "Preliminary Results on Performance Testing of a Turbocharged Rotary Combustion Engine" - Meng P. R., Rice W. J., Schock H. J., Pringle D.P. (1982). International Congress and Exposition. Detroit, Michigan, SAE
 - (4) "Computational Investigation of a new concept rotary engine" - Savvas Savvakis, Laboratory of Applied Thermodynamics, Department of Mechanical Engineering, Aristotle University of Thessaloniki, Greece, July 2011
 - (5) "Internal Combustion Engines : Applied Thermosciences" – Colin R. Ferguson, Allan T. Kirkpatrick, edited in Greek language by Associate Professor G.Ch. Koltsakis, Aristotle University of Thessaloniki, Grapholine, 2001
 - (6) "Atkinson Meets Otto: Why the Prius is so efficient" – Toyota Open Road Blog, Sept. 08, 2008, www.pressroom.toyota.com
 - (7) "Internal Combustion Engine Fundamentals" – John Heywood, April 1988, ISBN: 978-7086375
 - (8) "Internal Combustion Engines" – V.Ganesan, Second edition, Tata Mcgraw Hill, ISBN: 0-07-049457-6
-